OAK RIDGE NATIONAL LABORATORY
operated by
UNION CARBIDE CORPORATION
for the
U.S. ATOMIC ENERGY COMMISSION

ORNL-TM-293

HIGH-TEMPERATURE REACTIONS OF TYPE 304 STAINLESS STEEL IN LOW CONCENTRATIONS OF CARBON DIOXIDE AND CARBON MONOXIDE

H. Inouye

ORNL-TM-293

Copy

Contract No. W-7405-eng-26

METALS AND CERAMICS DIVISION

HIGH-TEMPERATURE REACTIONS OF TYPE 304 STAINLESS STEEL IN LOW CONCENTRATIONS OF CARBON DIOXIDE AND CARBON MONOXIDE

H. Inouye

DATE ISSUED

AUG 2 9 1962

OAK RIDGE NATIONAL LABORATORY
Oak Ridge, Tennessee
operated by
UNION CARBIDE CORPORATION
for the
U. S. ATOMIC ENERGY COMMISSION

ABSTRACT

Compatibility studies of type 304 stainless steel in helium containing low concentrations of carbon monoxide and carbon dioxide were conducted as part of the fuel development program of the Experimental Gas-Cooled Reactor. The extent of the gas-metal reactions was determined in order to specify their allowable levels in the coolant.

The oxidation rates were insensitive to impurity concentrations between 0.0006–0.3 vol % in the temperature range 400–1000°C when P_{CO_2}/P_{CO} was less than 0.66. Ratios above this value resulted initially in a slow oxidation rate, as before, but was followed by an accelerated attack. The incubation period for this "break-away" varied with the P_{CO_2}/P_{CO} ratio and the pressure of the two gases. This phenomenon results from a protective oxide-gas reaction to form nonprotective Fe_3O_4. Under thermal cycling, Fe_3O_4 spalls and in service would introduce oxide particles into the coolant stream.

The oxidation reactions proceeded through a selective depletion of chromium from the alloy which increased the carbon solubility and depletion of nickel which led to the transformation of austenite to ferrite. Parabolic reaction rates were observed for the formation of the protective oxides. Arrhenius plots of rate constants versus $\frac{1}{T}$ indicated the presence of several oxides which was confirmed by other methods.

Carburization or decarburization reactions occurred coincidentally with oxidation and depended upon temperature and $(P_{CO})^2/P_{CO_2}$ and the P_{CO_2}/P_{CO}. Neither was detected below 600°C. Between 600–900°C, only carburization occurred and appeared to be mainly dependent on the temperature. Above 900°C, both carburization and decarburization occurred depending upon the $(P_{CO})^2/P_{CO_2}$ and the P_{CO_2}/P_{CO}. The interactions of the oxidizing and carburization reactions resulted in carbon maxima at a $(P_{CO})^2/P_{CO_2}$ ratio of 0.227.

This investigation indicates that it may be impractical or unnecessary to reduce impurity gases to levels which do not cause surface reactions. It is concluded that undesirable oxidation and carburization reactions can be eliminated by controlling the ratios of the impurity gases.

HIGH-TEMPERATURE REACTIONS OF TYPE 304 STAINLESS STEEL IN LOW CONCENTRATIONS OF CARBON DIOXIDE AND CARBON MONOXIDE

H. Inouye

INTRODUCTION

Type 304 stainless steel (18 Cr–12 Ni–0.1 C–bal Fe) was selected as the clad for the fuel elements of the Experimental Gas-Cooled Reactor (EGCR). As presently designed, the fuel elements will be exposed to helium at 315 psia for a scheduled lifetime of approximately 25,000 hr, or 3 years. Due to desorption of gases from the graphite moderator and to anticipated system leaks, the helium coolant is expected to contain low concentrations of CO, CO_2, H_2, H_2O, N_2, and CH_4 as the major impurities. The metal surface temperatures for the 0.710-in.-ID × 0.020-in.-wall tubing are estimated to be between 200 and 1000°C.

Since the major elements in type 304 stainless steel are iron, chromium, nickel, and carbon, each exhibiting various degrees of reactivity with CO and CO_2, selective reactions resulting in oxidation, carburization, and decarburization were postulated to occur depending on the composition of the impure helium. Inasmuch as the useful life of the clad will be influenced by the above reactions, it was necessary to determine the severity and types of reaction occurring and to indicate the extent of control attainable over these reactions by controlling the composition of the atmosphere.

This paper presents the results of a detailed investigation of the reactions of the alloy with low concentrations of CO and CO_2. The purpose of the investigation was to develop the basic principles governing the

corrosion phenomena in CO and CO_2 so that the interacting effects of the other listed gases could be determined by subsequent tests. In addition, experimental conditions were selected which would establish those atmospheres that are both compatible and incompatible with the clad. It was concluded that this approach was the most desirable way to establish the framework for the selection of advanced fuel element clads and a basis for the purification of the helium coolant.

BASIC PRINCIPLES

It would appear that the velocity of the helium and the concentration of the impurity gases therein would be the important variables affecting their reactions with the clad. It is pointed out, however, that the characteristic properties of the reaction products are the most important variable since they form an intermediate barrier between the metal and the gases within a short time at high temperatures.

When the reaction product forms an effective barrier, its presence is detected by a reaction that decreases in extent with time, which results from the reaction rate being dependent upon the rate of diffusion of the reacting species through a reaction product that is increasing in thickness with time. The reaction rates observed for oxides that form protective layers are often parabolic and are affected primarily by temperature, time, and type of oxide on the surface. Pressure and velocity in this case have only a slight effect.

If the reaction results in the formation of a nonprotective reaction product, the extent of reaction varies linearly or accelerates with time. The reaction rate in this case increases with gas pressure and velocity

since the rate-controlling reaction occurs at the gas interface, which may be the metal or a reaction product.

The principal problem therefore reduces to determining those gas conditions which will result in the formation of protective reaction products and to maintaining the gases within this range through purification.

PREVIOUS INVESTIGATIONS

Bockros and Shoemaker [1] investigated the compatibility of numerous high-temperature alloys, including types 430 and 316 stainless steels in helium containing CO and CO_2. For temperatures up to 927°C and times up to 500 hr, the extent of carburization was equivalent for $P_{CO} + P_{CO_2}$ concentrations of 2×10^{-4} or 1×10^{-2} atm and increased with time and temperature. Carbon monoxide at 1 atm was slightly more carburizing toward type 316 stainless steel than were the CO + CO_2 atmospheres at 860°C. The oxide reaction products in these tests were either the spinels or spinels and Cr_2O_3. Maximum changes in the weight were observed at 760°C.

Other investigations related to the present study were concerned with the corrosion of conventional heat-resistant nickel-base alloys and the stainless steels in CO_2. In 100-hr tests at 982°C Pessl [2] determined that Hastelloys X and N were the most corrosion-resistant alloys in 1 atm of CO_2. Bockros [3] found that the stainless steels were severely oxidized at 948°C and moderately at 816°C in 1000 psi CO_2. Three austenitic steels that he evaluated showed a weight gain of between 1.3 to 2.5 mg/cm^2 at 816°C for test times of 1008 hr.

A more detailed study by Draycott [4] showed that the reaction rates of type 321 stainless steel (18 Cr–12 Ni–titanium stabilized) with CO_2 were sensitive to the method of surface preparation, increasing with gas pressure, gas velocity, and moisture between 550 and 700°C. The extent of reaction decreased with time, being on the order of 0.16 to 0.30 mg/cm^2 depending on the CO_2 pressure (78 to 225 psi) for exposure times of 750 hr at 695°C. The oxide reaction products were Cr_2O_3, Fe_2O_3, Fe_3O_4, and various spinels ($NiO\cdot$, $MnO\cdot$, $FeO\cdot Cr_2O_3$). Carburization was not observed although the sigma phase was identified as a precipitated phase.

An analysis of the data in the cited literature indicates that carburization and oxidation are not serious problems up to about 700°C. Inasmuch as temperatures in excess of 700°C are expected for the fuel elements of the EGCR, the CO and CO_2 impurities in helium would apparently present a problem of compatibility.

EXPERIMENTAL PROCEDURE

The experimental tests were patterned to approximate the steady-state service conditions of the reactor (except for irradiation), with the provision that the impurities would be controlled to various selected concentrations that would simulate the operation of a gas purification system. The experimental difficulties associated with high-pressure, high-velocity, and high-temperature testing and the conclusion that pressure and velocity effects of the impurities in helium would be insignificant under certain conditions made it advantageous to conduct the tests in controlled concentrations of CO and CO_2 at various temperatures, using helium only as the carrier gas at some convenient pressure. This

approach was based on the premise that helium would be totally inert with respect to its influence on the reactions between the clad and the active gases. For the purposes of this paper, the impurity concentrations are expressed as partial pressures P in atmospheres or as volume percent based upon 315 psia [(P/21.4) × 100 = volume percent].

The gas compositions selected for the compatibility tests were in the range of concentrations of CO and CO_2 that were considered to be compatible with the graphite at about 600°C. The CO_2 concentrations investigated ranged up to 2440 ppm and the CO + CO_2 concentrations ranged up to 3200 ppm.

The experimental apparatus, schematically shown in Fig. 1, was operated as a closed system with four furnaces, indicated by A, B, C, and D. The system was operated at a total helium plus impurity pressure of about 100 mm Hg and with the gases flowing, due to thermal convection in the pyrex and quartz tubes, in the direction indicated by the arrows. This pressure was selected to minimize the buoyant effect of the upward flowing gases on the specimen suspended from the spring.

The outer two furnaces, indicated by A and B, contained the test specimens. In furnace A, a 0.500-in.-OD × 0.002-in.-wall × $1\frac{1}{2}$-in.-long tubular specimen weighing approximately 1 g (approximately 40 cm^2) was suspended from the end of a 0.003-in.-diam platinum wire attached to a calibrated steel spring for rate measurements. In furnace B, 15 specimens were placed on separate platinum pans and arranged in a temperature gradient from about 400 to 1050°C. Ten of the specimen tubes were 0.500-in.-OD × 0.002-in.-wall × $\frac{1}{2}$-in. length and five were 0.710-in. OD × 0.020-in. wall × $\frac{1}{2}$-in. length.

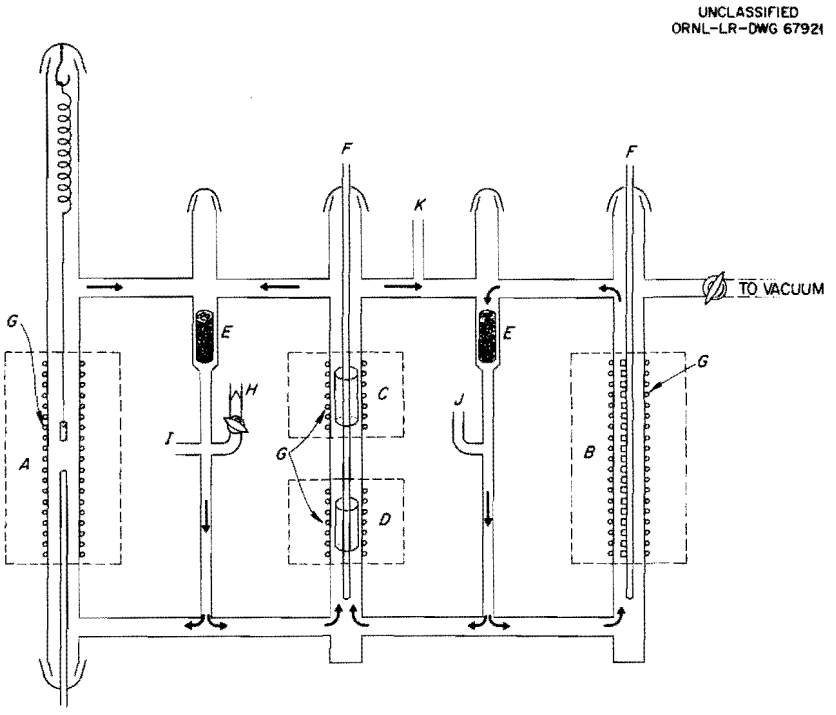

Fig. 1. Apparatus for Testing Metal Specimens in a Controlled Atmosphere of $CO-CO_2$.

Subsequent to evacuating the system to 10^{-5} mm Hg with all the furnaces at 300°C, the apparatus was filled with helium and the samples were brought to the reaction temperature. During the next 18 hr the gases in the system were analyzed at 15-min intervals to detect system leaks with a Beckman 320C gas chromatograph. When the system was determined to be leaktight, chemically pure $CaCO_3$ was decomposed in furnace D to generate CO_2, which was then reacted with Fe_3C (coiled iron wire containing 1% C) or graphite (cast iron chips) in furnace C to generate CO.* Although the above reactions were reversible and therefore self-regulating under isothermal conditions, the gases were analyzed and proper temperature adjustments of the generators were made to compensate for gases removed from or added to the system. The reported gas compositions represent a time-compensated average of at least 35 analyses selected as representative values during the run.

The weight changes of the specimens after testing were recorded to construct the curves showing the temperature dependence of the reaction rate in the particular atmosphere. In order to do this, it was assumed that the rate law governing the oxidation of the specimen in furnace A was the same for the specimens in furnace B when their weight changes were lower than that for the specimen in furnace A. For this reason, the rate measurements in furnace A were made at the highest temperature investigated.

---

*The equilibrium value of CO_2 was attained within 15 min at temperature, while 24 hr was required for the CO. Activated charcoal required approximately 200 hr to come to equilibrium and was therefore not used. When CO_2 atmospheres were desired, the CO generator was replaced with CuO pellets operating at 240°C.

The 0.002-in.-thick specimens were analyzed for carbon with and without the oxide to establish the location of the carbon. Sections of the 0.020-in.-thick specimen were used to identify the reaction products and to prepare metallographic specimens.

The chemical compositions of the two lots of tubing used for this study are given in Table I.

RESULTS

Oxidation Reactions in CO_2

The reaction rates of type 304 stainless steel with three concentrations of CO_2 at 760°C are shown in Fig. 2. The tests at 0.6 and 6.0 ppm CO_2 were conducted with only CO_2 as the atmosphere in a dynamic vacuum; the test at 2440 ppm CO_2 was conducted in the presence of helium at a pressure of 100 mm Hg in the apparatus shown in Fig. 1, and its parabolic rate constant was used to calculate the curve shown in Fig. 2. For each test a short period of rapid oxidation was followed by longer periods of slower oxidation. This series of tests showed that an increase in the CO_2 pressure by a factor of about 4000 decreased the extent of reaction by about 50%. The oxide phases resulting from these tests were a magnetic orthorhombic phase of the composition $3Cr_2O_3 \cdot Fe_2O_3$ and a spinel of the composition $MnO \cdot Cr_2O_3$.

In the normal course of checking the weight changes indicated by the calibrated steel spring with the before and after sample weights on an analytical balance, it was observed that when the weight changes exceeded about 0.3 mg/cm^2 the oxide spalled off the specimen upon cooling to room temperature. The apparent oxidation based on before and after weights

Table I. Composition of Type 304 Stainless Steel Tubing

Heat A Tubing: 0.500-in. OD × 0.002-in. wall
Heat B Tubing: 0.710-in. OD × 0.020-in. wall

Element	Composition (wt %)	
	Heat A	Heat B
Cr	18.30	18.22
Ni	10.44	10.32
Mn	1.63	1.91
Si	0.50	0.50
C	0.075	0.065
Mo	0.13	0.17

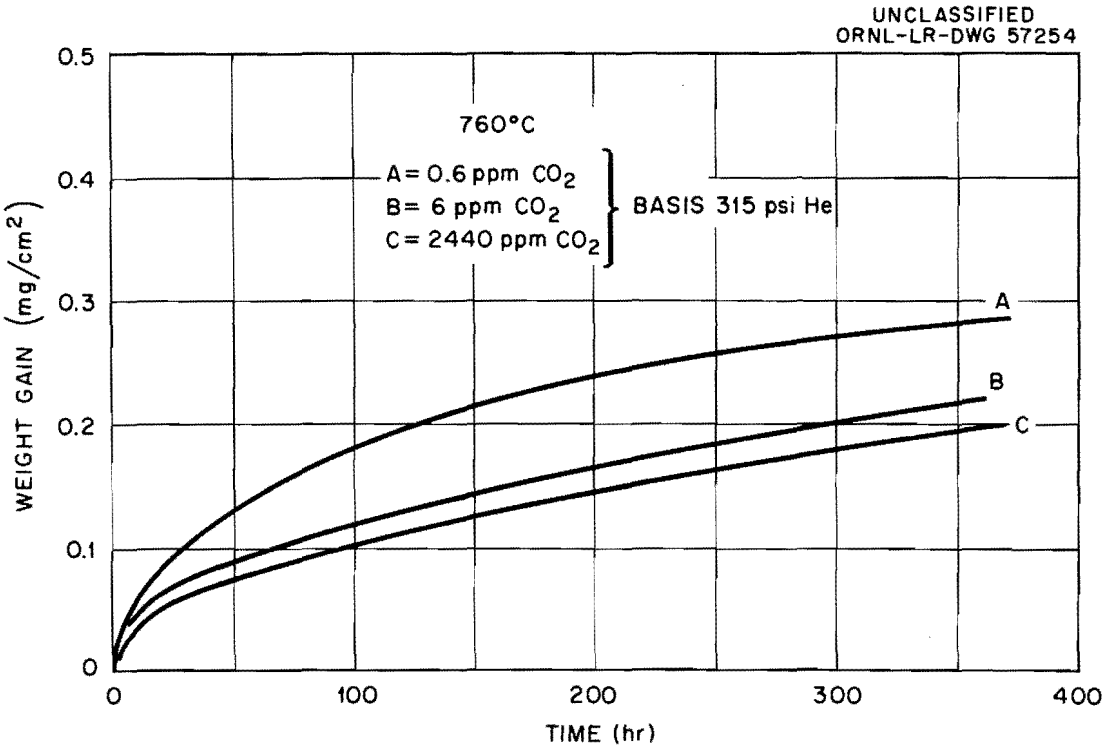

Fig. 2. Oxidation of Type 304 Stainless Steel in CO_2 at 760°C.

therefore resulted in either low or negative weight changes. A specific test was conducted to examine in more detail the character of the spalling phenonomenon. The specimen was oxidized in CO_2 to a weight increase of 0.584 mg/cm^2 at 982°C as indicated by the calibrated spring. The weight change was then determined after cooling in 50°C intervals to room temperature. The weight loss of the specimen with temperature is shown in Fig. 3. At room temperature the specimen showed a very thin oxide layer and an apparent weight increase of 0.04 mg/cm^2.

The reaction rates of the alloy with two concentrations of CO_2 at 982°C are shown in Fig. 4. In contrast to the tests at 760°C, the extent of reaction increased with the CO_2 pressure. At the higher pressure, the initially decreasing rate of reaction exhibited a transition to a linear or an accelerated rate after about 125 hr and at a weight increase of 1.8 mg/cm^2. The weight increase of the specimen exposed to the lower CO_2 pressure varied linearly with time between 20 and 400 hr, and thereafter decreased perceptibly with time up to 840 hr.

Table II lists the weight changes, the reaction products, and a brief description of the reaction products for specimens exposed to 0.244 vol % CO_2 in the range 434 to 992°C. Of particular interest was the growth of Fe_3O_4 whiskers from the edges of the 0.020-in.-thick specimens oxidized at temperatures above 935°C. A 10X photograph of a representative specimen is shown in Fig. 5.

To illustrate the temperature dependence of the reaction rates, it was assumed that those specimens with weight gains of less than 1.8 mg/cm^2 did not exhibit a "breakaway" phenomenon and were therefore governed by the parabolic rate law. On this basis the parabolic rate constants were

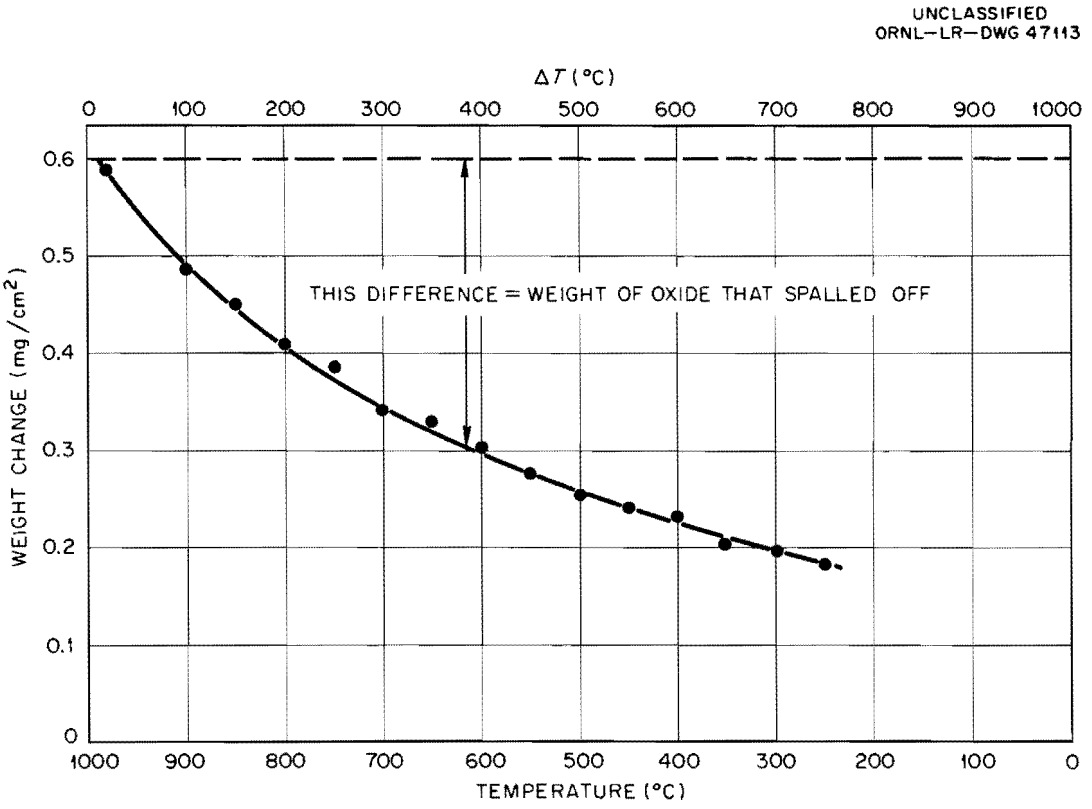

Fig. 3. Weight Losses Observed During Cooling of Type 304 Stainless Steel Oxidized in 6 ppm CO_2 at 982°C.

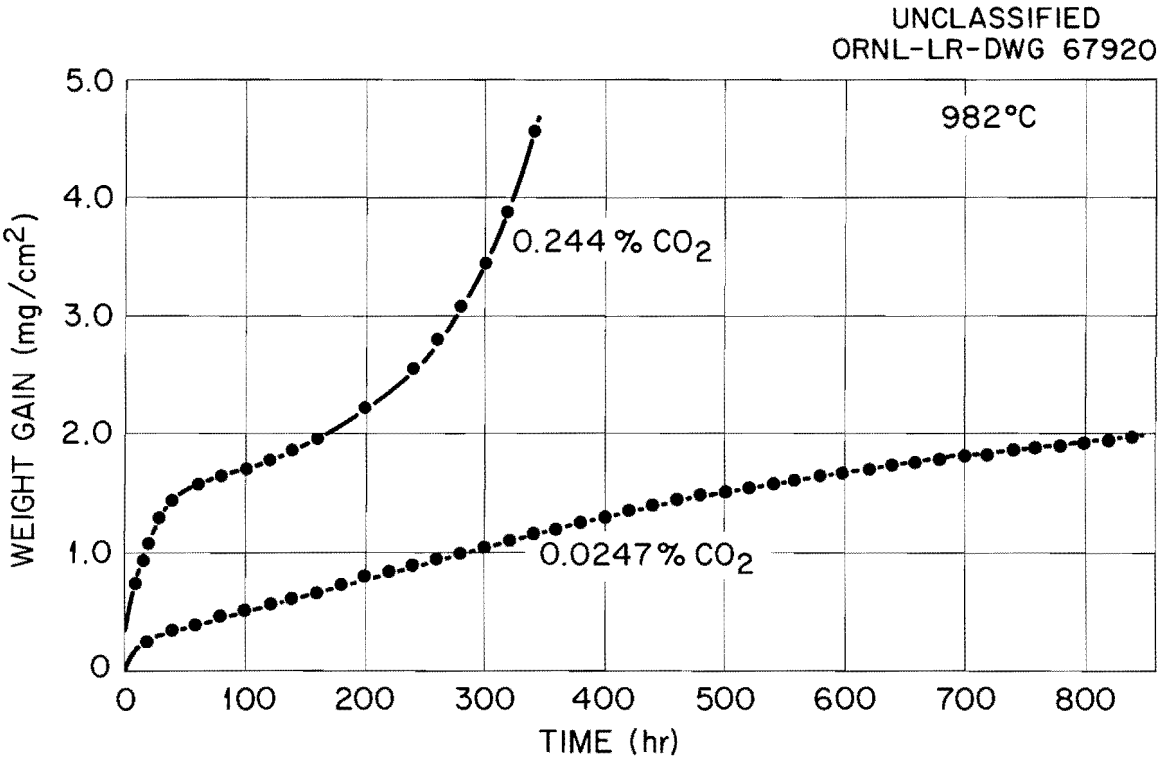

Fig. 4. Oxidation Rates of Type 304 Stainless Steel in CO_2 at 982°C.

Table II. Effect of Temperature on the Oxidation of Type 304 Stainless Steel Exposed to 0.244% CO_2 for 818 hr

Test Temperature (°C)[a]	Weight Gain (mg/cm^2)	Appearance of Test Specimen	Oxide Phase[b]
434	0.11	Blue interference color	
603	0.19	Mottled gray-brown powdery oxide	Fe_2O_3 (M); Cr_2O_3 (W)
670	0.23	Mottled gray-brown powdery oxide	
680	0.24	Mottled gray-brown powdery oxide	
695	0.27	Mottled gray-brown powdery oxide	
725	0.22	Nonadherent brown powdery oxide	
764	0.30	Nonadherent brown powdery oxide	
794	0.35	Nonadherent brown powdery oxide	Fe_3O_4 (M); MnO (M); Cr_2O_3 (M)
816	0.41	Gray-tan powdery oxide	
879	0.67	Gray-tan powdery oxide	MnO (S); Cr_2O_3 (M); Fe_3O_4 (M)
920	1.12	Black crystalline oxide over gray-brown oxide	
935	1.34	Black crystalline oxide over gray-brown oxide	Fe_3O_4 (S); Cr_2O_3 (S); MnO (M)
975	7.43	Black oxide whiskers over gray-brown oxide	Fe_3O_4 (S)
977	6.32	Black oxide whiskers over gray-brown oxide	Fe_3O_4 (S)
992	13.92	Black oxide whiskers over gray-brown oxide	Fe_3O_4 (S)

[a] Specimens up to 879°C were 0.002 in. thick; above 879°C, 0.020 in. thick.

[b] α-iron was a strong x-ray component up to 935°C; above 935°C a strong body-centered cubic phase (probably Δ-iron) was present. Letters in parentheses indicate x-ray intensities: S, strong; M, medium, W, weak.

Unclassified
Y-39545

Fig. 5. Photograph of Fe_3O_4 Whiskers on Type 304 Stainless Steel Exposed for 818 hr to 0.244% CO_2 at 977°C.

calculated and their logarithms plotted vs 1/T as shown in Fig. 6, together with the oxides identified at the corresponding temperatures. Although the weight gain data shown in Table II indicate that the parabolic rate law did not apply at test temperatures above 935°C, the rate constants were calculated to show the relationship between the oxidation rate constants and the corresponding reaction products.

Oxidation Reactions in CO-CO_2

The reaction rate of type 304 stainless steel in a CO-CO_2 atmosphere in which the CO_2/CO ratio was 0.669 is shown in Fig. 7. As in the case of the test in CO_2 at 0.244%, the specimen in this test exhibited a breakaway reaction at a weight gain of 1.8 mg/cm^2 in about 500 hr and the oxidation continued at an accelerated rate for 1390 hr. The specimen after testing showed a blistered surface composed of a black oxide over a green oxide. As in the tests in CO_2, the oxides on the specimens at temperatures between 710 and 1010°C were not adherent and the specimens showed the presence of two oxides, as judged by their color.

The effect of the CO_2/CO ratios at comparable concentrations of $CO + CO_2$ and 982°C is shown in Fig. 8. These data show that the breakaway reaction will occur in CO_2 and in CO-CO_2 atmospheres at a CO_2/CO value of 0.669.

Reaction rates for type 304 stainless steel at two CO_2/CO ratios are shown in Fig. 9. The equations for the rate curves are of the form $\Delta W = kt^n$, where ΔW is the weight gain in mg/cm^2, t is the reaction time in hours, and n and k are constants. As shown in Table III, the average values for n and k are 0.504 and 0.071, which clearly meets the parabolic reaction rate requirement. It should be noted that variations in

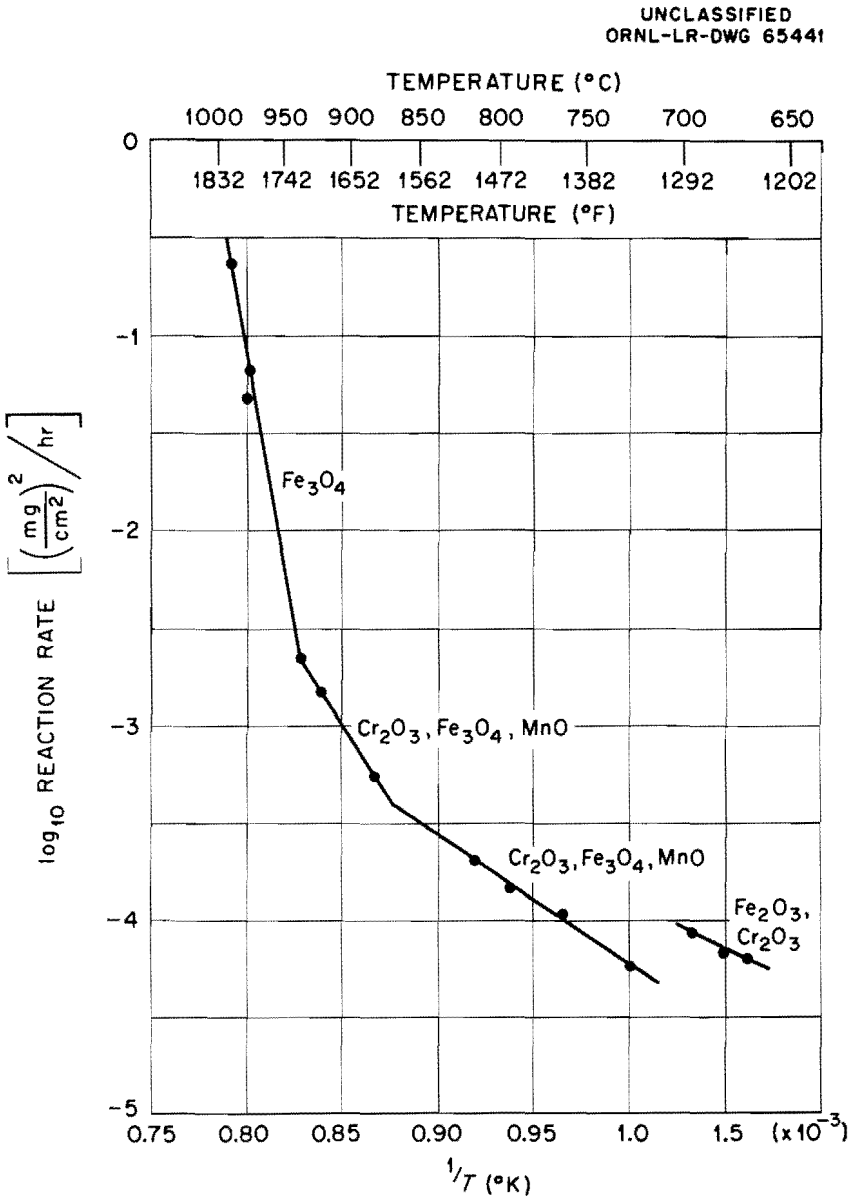

Fig. 6. Temperature Dependence of the Reaction Rate Constant of Type 304 Stainless Steel Oxidized in 0.244% CO_2.

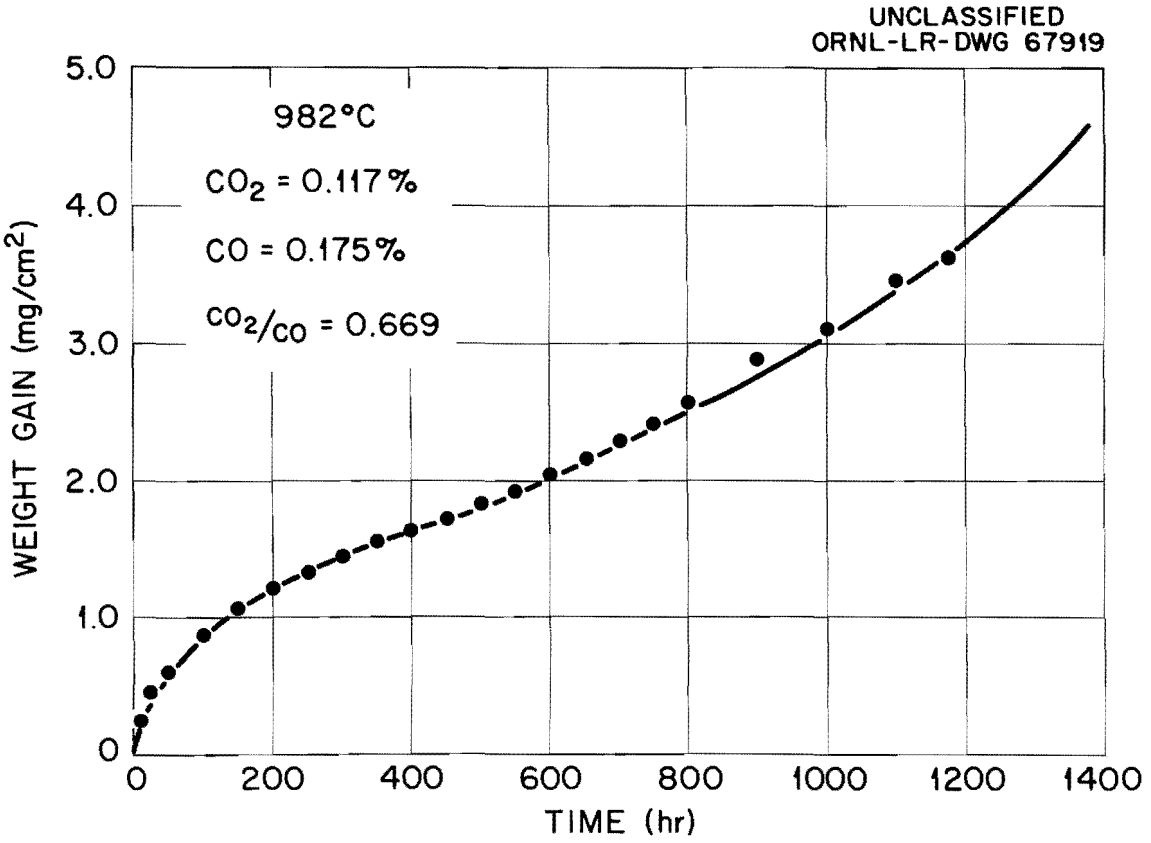

Fig. 7. Oxidation Rate of Type 304 Stainless Steel at P_{CO_2}/P_{CO} Ratio of 0.669 and 982°C.

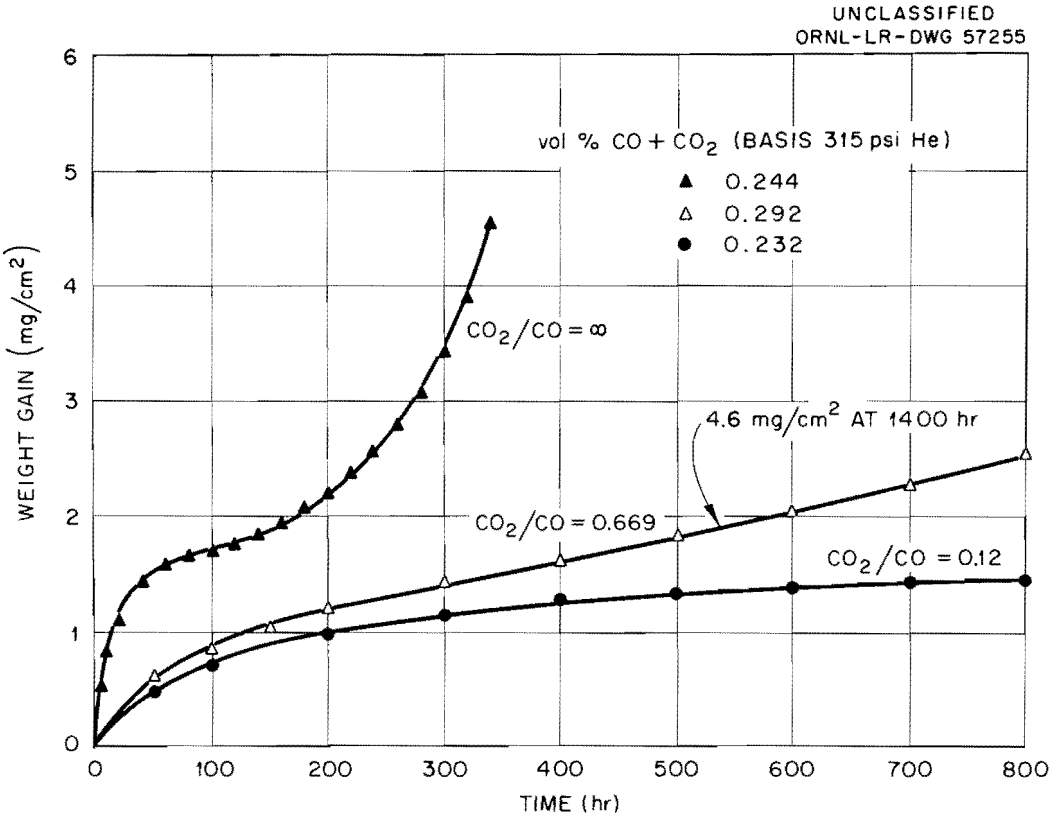

Fig. 8. Effect of the P_{CO_2}/P_{CO} Ratio on the Oxidation of Type 304 Stainless Steel at 982°C.

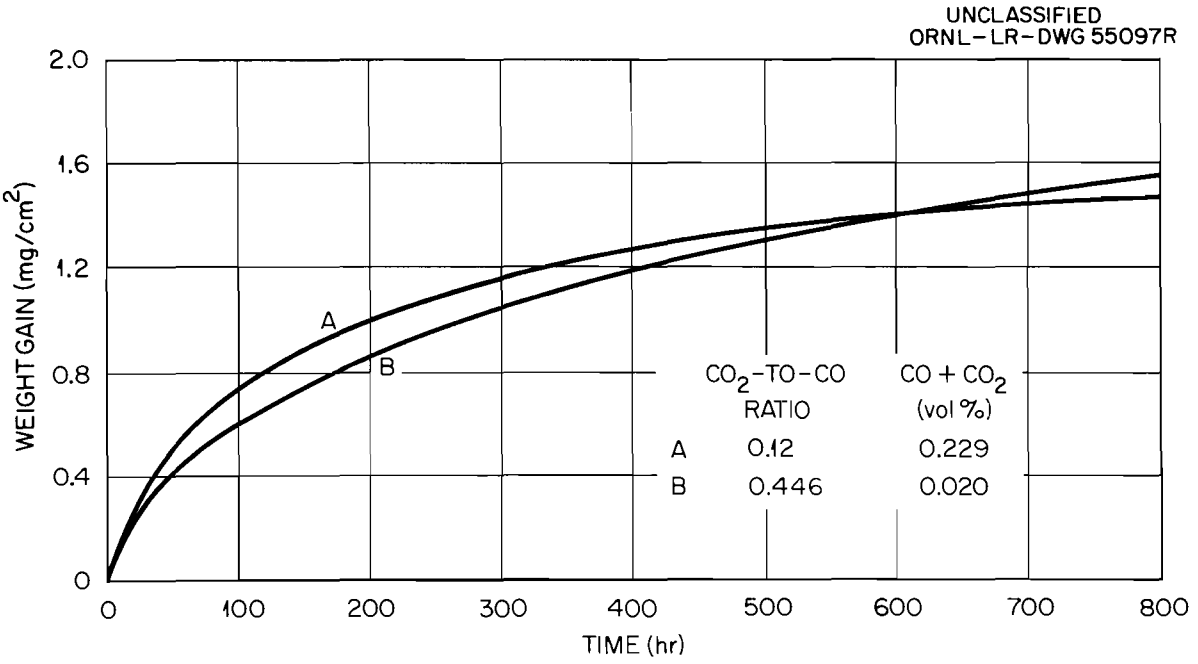

Fig. 9. Representative Rate Curves for the Oxidation of Type 304 Stainless Steel at 982°C and P_{CO_2}/P_{CO} Ratios Less Than 0.446.

Table III. Reaction Rates of Type 304 Stainless Steel with Various P_{CO_2}/P_{CO} Ratios at 982°C

Test Time (hr)	Concentration (%)			P_{CO_2}/P_{CO}	k	n	Weight Gain (mg/cm^2. 700 hr)
	CO_2	CO	$CO + CO_2$				
192	0.0056	0.312	0.3176	0.018	0.069	0.567	
839	0.0077	0.177	0.1847	0.043	0.077	0.462	1.39
318	0.0100	0.133	0.1430	0.089	0.086	0.502	
841	0.0117	0.1112	0.1229	0.105	0.064	0.477	1.43
820	0.0248	0.207	0.2318	0.120	0.061	0.533	1.42
720	0.0063	0.0141	0.0204	0.446	0.066	0.481	1.44
				Av	0.071	0.504	

the CO + CO_2 concentration by a factor of about 15:1 and variations of 25:1 in the CO_2/CO ratio do not result in any difference in the reaction rates. The concentration range represented was between 204 and 3176 ppm CO + CO_2 and the relative percentages of CO_2 were between 2 and 55% (45 and 98% CO).

The effect of temperature on the reaction rate constant for three gas mixtures is shown in Fig. 10. In general, the gas composition had little effect on the reaction rates above about 850°C (also apparent from the data in Table III). Below this temperature, the reaction rate constant increased as the CO_2/CO ratio was decreased. The oxide phases for the test at a CO_2/CO ratio of 0.12 were a cubic spinel phase and Cr_2O_3, with the Cr_2O_3 lines being weaker below 856°C. For the test conducted at a CO_2/CO ratio of 0.043, Cr_2O_3 was a strong phase at all temperatures and a strong spinel-like structure with a unit cell size of 8.42 A, identified as Fe_3O_4, was observed. In both tests a ferritic phase was also a major reaction product.

Carburization and Decarburization of Type 304 Stainless Steel in CO_2 and in CO-CO_2

The effect of CO_2 on the carbon content of type 304 stainless steel specimens after about 800 hr of exposure is shown in Fig. 11. The results indicated that CO_2 is neither carburizing nor decarburizing up to about 700°C, is carburizing up to 875°C, and is decarburizing above 875°C. The maximum carbon content of 0.23 wt % was observed at about 880°C.

A similar observation was noted for atmospheres of CO-CO_2 (Fig. 12). In these tests carburization commenced at about 650°C and increased as the $(P_{CO})^2/P_{CO_2}$ ratio was increased. A maximum content of 0.17 wt % C was

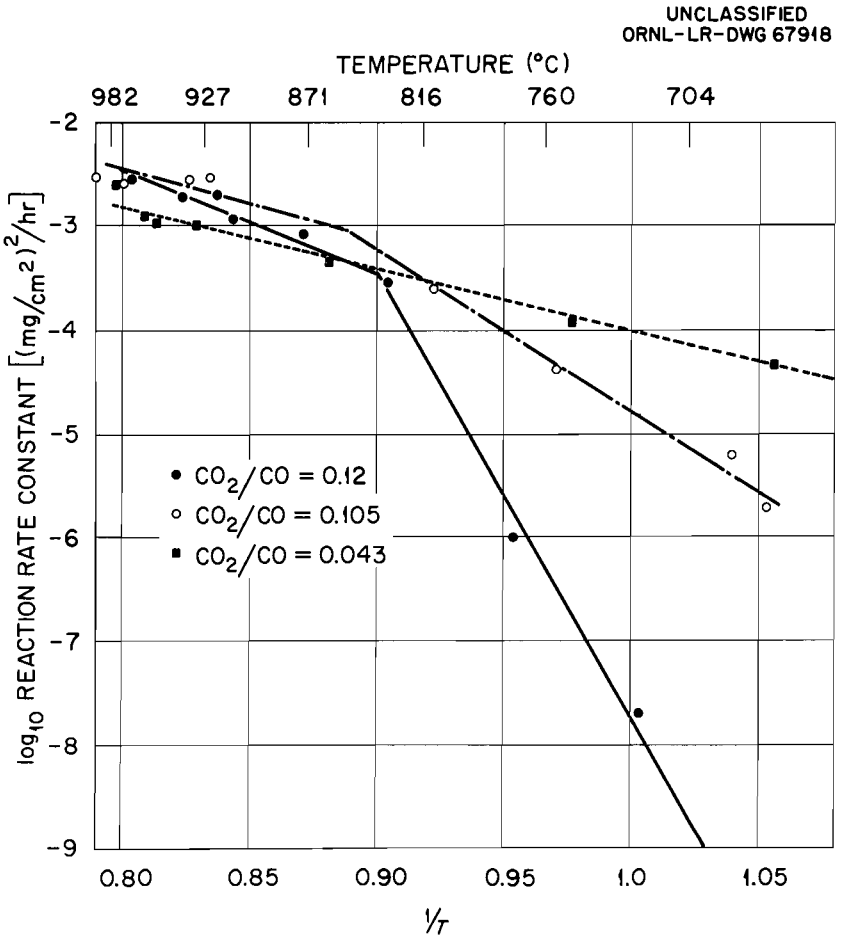

Fig. 10. Temperature Dependence of the Reaction Rate Constants on Temperature and the P_{CO_2}/P_{CO} Ratio.

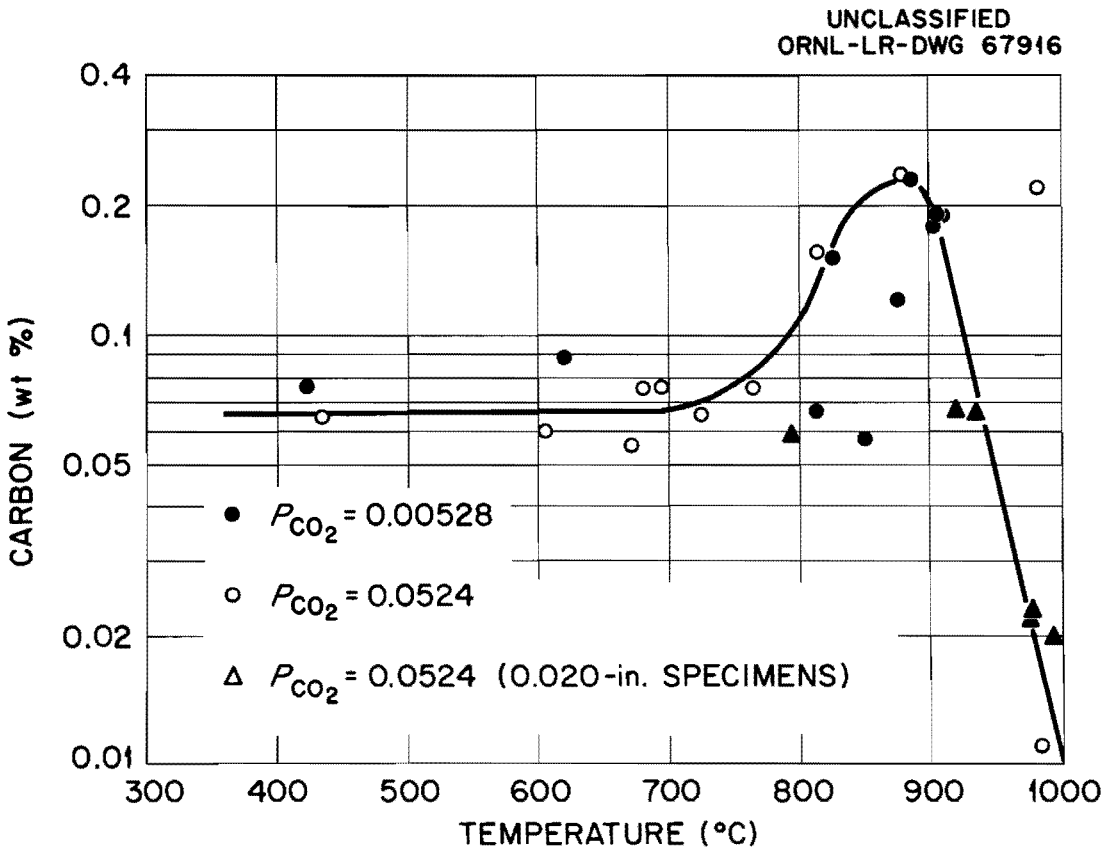

Fig. 11. Effects of Temperature and CO_2 on the Carbon Content of Type 304 Stainless Steel.

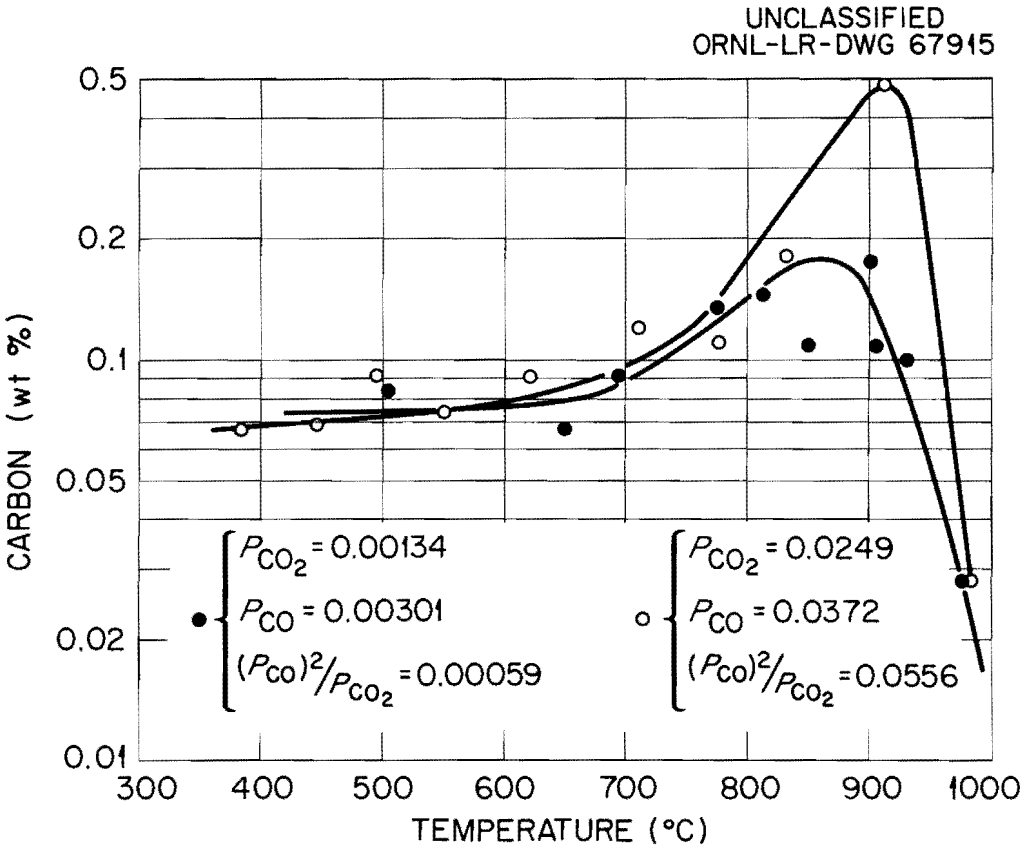

Fig. 12. Effects of Temperature and Intermediate $(P_{CO})^2/P_{CO_2}$ Ratios on the Carbon Content of Type 304 Stainless Steel.

indicated for the test at a $(P_{CO})^2/P_{CO_2}$ value of 5.9×10^{-4} at 850°C, while 0.39 wt % C was observed for a value of $(P_{CO})^2/P_{CO_2}$ of 0.055 at 910°C.

In atmospheres higher in CO content, only carburization was observed. As shown by Fig. 13, carburization occurred above 600°C, increased with temperature, passed through a maximum carbon content, then decreased with further increases in temperature. In contrast to the effect of $(P_{CO})^2/P_{CO_2}$ noted in Fig. 12, carburization in these tests decreased with increases in this ratio for the compositions studied. In addition, the maximum carbon contents were displaced to lower temperatures as the $(P_{CO})^2/P_{CO_2}$ was increased. A summary of the effect of the $(P_{CO})^2/P_{CO_2}$ ratio on the carbon content of type 304 stainless steel is given by the curves in Fig. 14, where the isotherms indicate a peak carburizing atmosphere at a $(P_{CO})^2/P_{CO_2}$ value of about 0.2.

Metallography

The microstructure of type 304 stainless steel exposed to CO_2 at 876°C is shown in Fig. 15. The large oxide patch represents areas of severe oxidation to a depth of about 0.001 in., sufficient concentration to give the metal interface an uneven appearance. On the basis of the x-ray data, the oxide patch was identified as predominantly Fe_3O_4. The metallic phase within the oxide was considered to be either unoxidized particles of the specimen or nickel deposited from the plating bath that was used to preserve the surface. The absence of particles outlining the grain boundaries to a depth of about 0.003 in. from the surface indicated that the alloy had been decarburized.

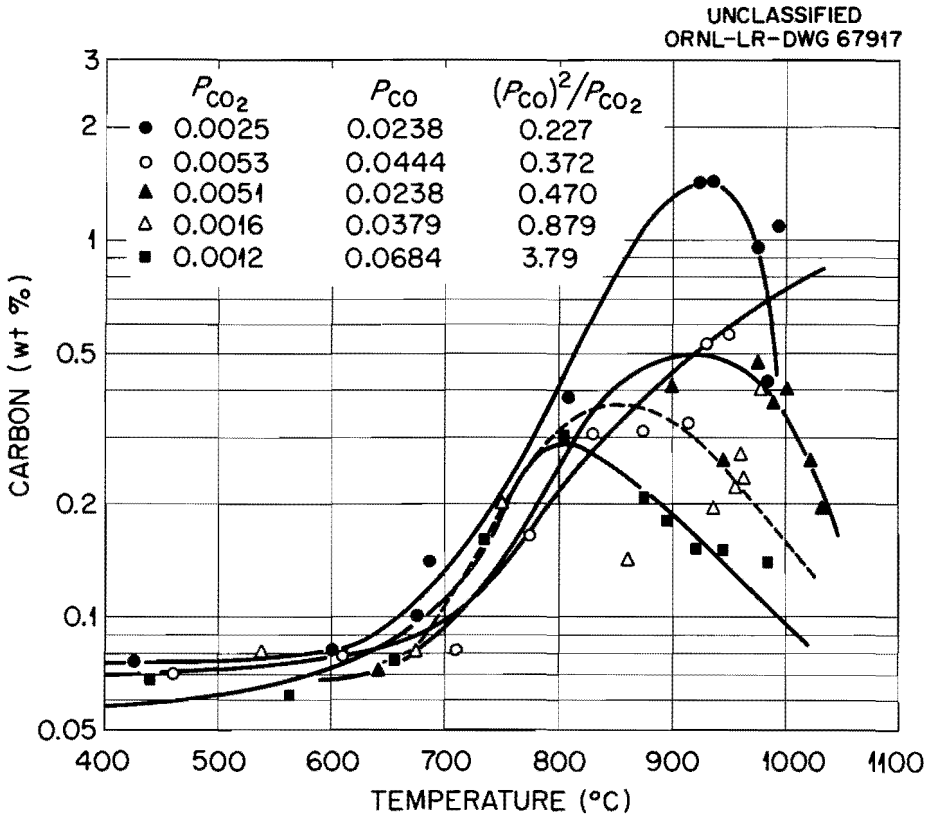

Fig. 13. Effects of Temperature and High $(P_{CO})^2/P_{CO_2}$ Ratios on the Carbon Content of Type 304 Stainless Steel.

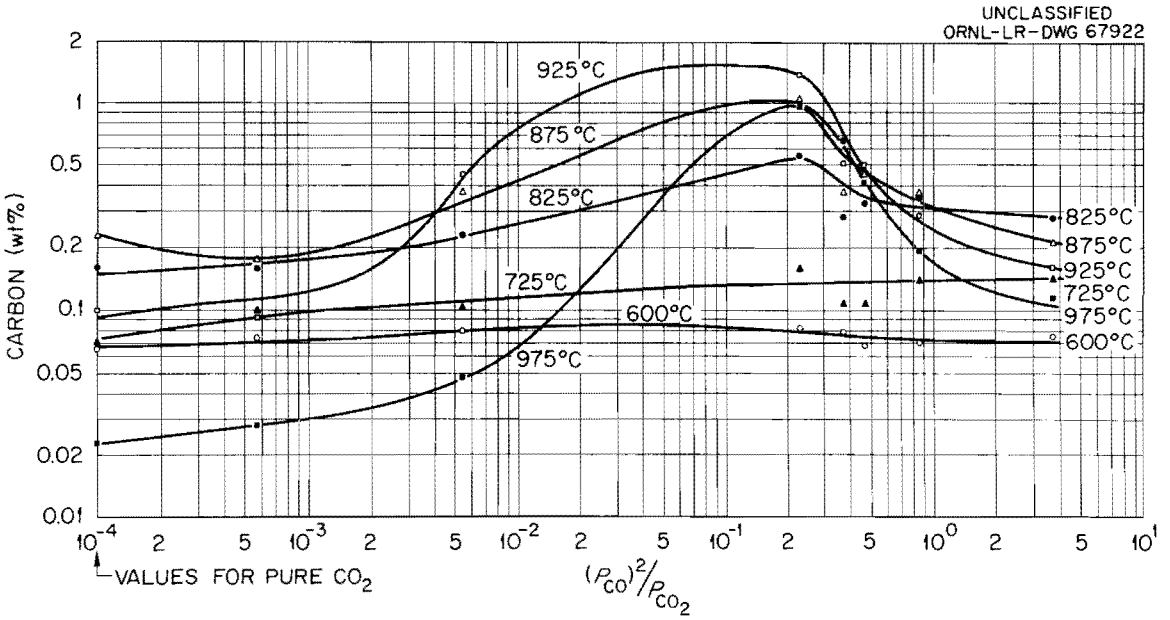

Fig. 14. Effect of $(P_{CO})^2/P_{CO_2}$ on the Carbon Content of Type 304 Stainless Steel.

Fig. 15. Photomicrograph of Type 304 Stainless Steel Oxidized for 840 hr in 0.0247% CO_2 at 876°C. Etchant: glyceria regia. 500X.

A typical microstructure of specimens exposed to CO-CO_2 atmospheres is shown in Fig. 16. Although oxidation was more uniform than in the CO_2 tests, isolated oxide islands were present to a depth of about 0.003 in., while a different type of oxide was apparent as a grain boundary phase to a depth of 0.001 to 0.002 in. The same specimen etched to bring out the grain boundary precipitates is shown in Fig. 17. The absence of particles outlining grain boundaries at the metal interface indicated that decarburization had occurred. Figure 18 illustrates the details of the microstructure of specimens oxidized at the highest temperatures. The oxides at the surface are spinels and Cr_2O_3, while within the metal near the surface ferrite and oxides outlining grain boundaries are apparent.

The microstructure of a specimen exposed at 489°C is shown in Fig. 19. The surface effects noted at 489°C are visibly less than at 955°C, but the carbide precipitates extend to the metal surface.

In atmospheres still higher in CO ($P_{CO_2}/P_{CO} < 0.04$), green crystallites were present at the metal-oxide interface and also extended into the metal at the grain boundaries. This layer varied in thickness and was topped by a dark-gray brittle phase extending almost to the gas interface. Individual green crystals and islands of green crystallites projected into and through the gray layer to the specimen surface. The surface was covered with a velvety-green oxide. X-ray and electron diffraction analyses of these phases indicated that Cr_2O_3 and Fe_3O_4 were the major phases. Within the alloy near the metal-oxide interface, ferrite was outlined to a depth of about 0.001 in. The microstructure was similar to that in Fig. 18.

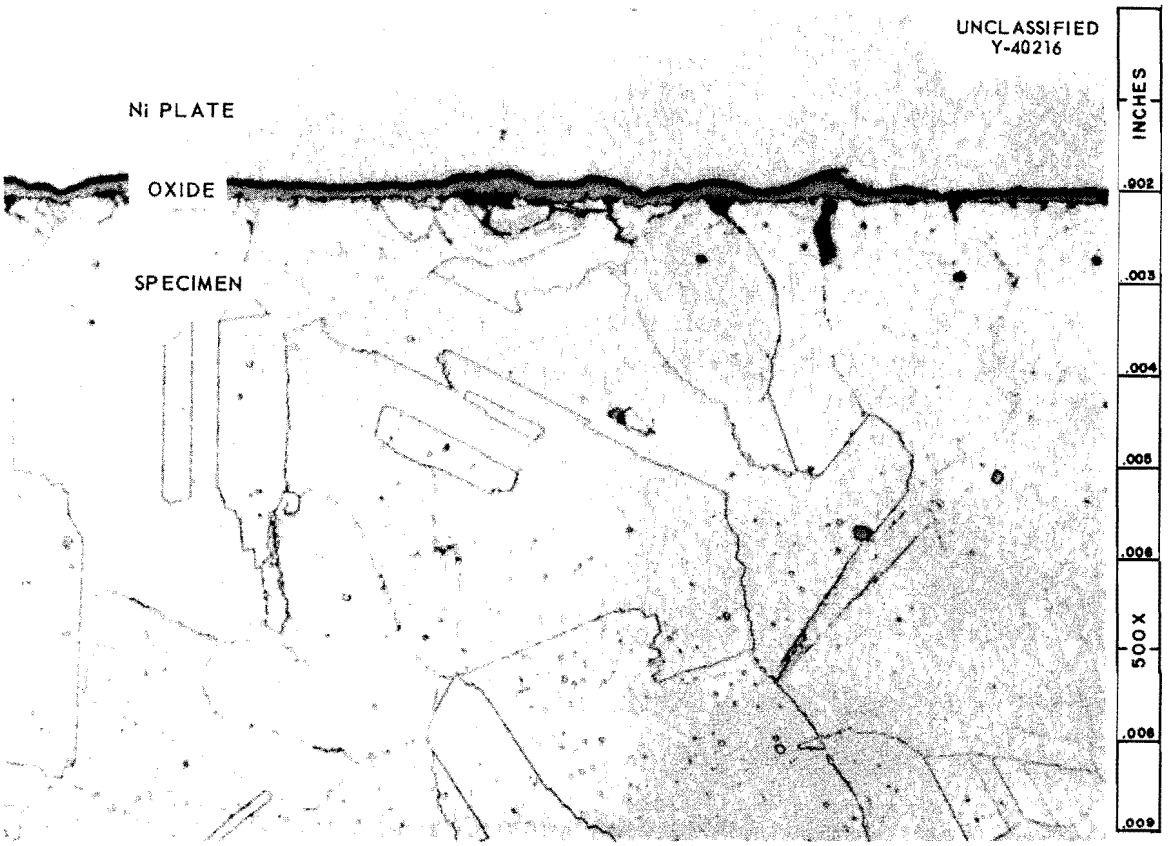

Fig. 16. Microstructure of Type 304 Stainless Steel Exposed for 820 hr at 858°C to an Atmosphere Where $P_{CO_2}/P_{CO} = 0.12$ and $(P_{CO})^2/P_{CO} = 0.372$.

Fig. 17. Microstructure of Type 304 Stainless Steel Exposed for 820 hr at 858°C to an Atmosphere Where P_{CO_2}/P_{CO} = 0.12 and $(P_{CO})^2/P_{CO_2}$ = 0.372. Etched to show carbides.

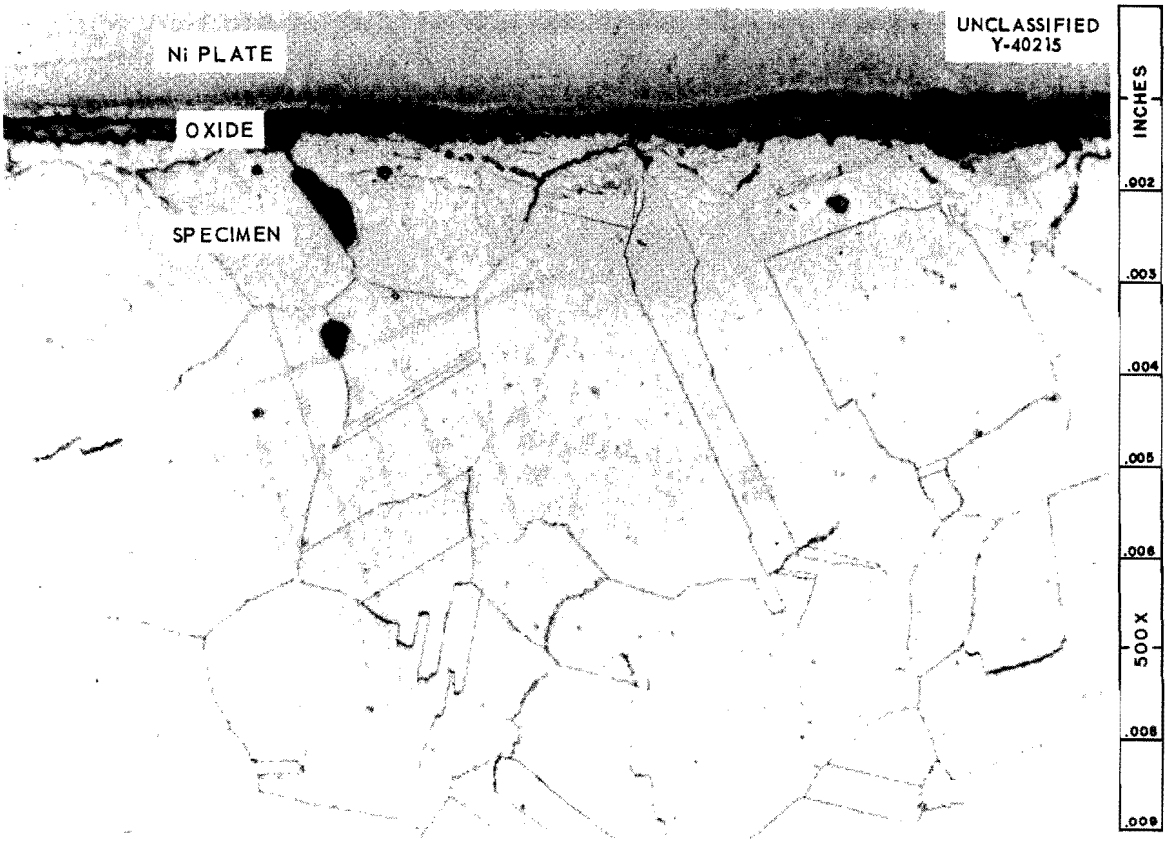

Fig. 18. Microstructure of Type 304 Stainless Steel Exposed for 820 hr at 955°C to an Atmosphere Where P_{CO_2}/P_{CO} = 0.12 and $(P_{CO})^2/P_{CO}$ = 0.372.

Fig. 19. Microstructure of Type 304 Stainless Steel Exposed for 820 hr at 489°C to an Atmosphere Where $P_{CO_2}/P_{CO} = 0.12$ and $(P_{CO})^2/P_{CO} = 0.372$.

DISCUSSION

Oxidation Reactions in CO and CO_2

The results showed that both CO and CO_2 oxidize type 304 stainless steel in a manner that depends principally on their ratio because of the presence of several elements in the alloy that exhibit varying degrees of reactivity with the gases. Therefore it was expected that the P_{CO_2}/P_{CO} ratio as well as temperature and time would influence the reaction rates.

When the atmosphere was oxidizing toward all the elements in the alloy, their corresponding oxides also appeared as the reaction products. This was illustrated by the tests conducted in CO_2 in which at least four oxides were observed at the various temperatures (see Table II). The degree to which these oxide layers protected the substrate metal depended upon the type of oxide (as shown in Fig. 6). The transition in the reaction rate constant at about 700°C was attributed to the appearance of new phases, while differences in the concentrations of Cr_2O_3, Fe_3O_4, and MnO were thought to have caused the inflection at about 875°C. The third inflection, at 935°C, was attributed to the disappearance of continuous layers of Cr_2O_3 and MnO (935°C was approximately the temperature at which Bockros observed excessive oxidation in CO_2 at 1000 psi pressure). The Fe_3O_4 layer appeared to be least protective. The order in which the various oxides were formed, as indicated by the color of the layers (Table II), suggested that the outer layer was Fe_3O_4 (Fe_2O_3 at the lower temperatures) and that the inner layers were MnO and Cr_2O_3. These three oxides are apparently the stable phases that resulted from the decomposition of $MnO \cdot Cr_2O_3$ and $3Cr_2O_3 \cdot Fe_2O_3$, which were identified after the short-time test in CO_2.

The increase in the oxidation rate with the CO_2 pressure and the occurrence of the breakaway phenomenon (Fig. 4) would require the rate-controlling reaction to occur at the gas interface. The rate curve observed for the test at 0.244% CO_2 suggested that the principal reaction accounting for the breakaway reaction occurred between CO_2 and an unidentified protective oxide to form the nonprotective oxide Fe_3O_4. However, since the oxide spalled in certain instances to reveal an adherent suboxide and at other times to reveal the base alloy, the breakaway reaction could have resulted from a reaction at the metal-oxide interface as well. The oxide that was associated with the breakaway reaction and that spalled (upon cooling of the oxidized specimens) was identified as Fe_3O_4.

The reactions involving the breakaway phenomenon are intimately associated with the reaction which forms nonprotective Fe_3O_4. The possible reactions are (1) the decomposition, or oxidation, of $3Cr_2O_3 \cdot Fe_2O_3$, which is apparently a transition phase, (2) the oxidation of the spinels such as $FeO \cdot Cr_2O_3$, (3) the formation of Fe_3O_4 directly from the reaction of Fe with CO_2, and (4) the formation of FeO from a reaction of Fe with CO_2 and its subsequent transformation to Fe and Fe_3O_4 upon cooling.

The evidence for reaction (1) being a possible reaction is that $3Cr_2O_3 \cdot Fe_2O_3$ was not a stable phase after 300 hr. Furthermore, it was observed (Table II) that a suboxide, gray-brown in color, was present in those specimens that exhibited the breakaway, which would tend to support the concept that the breakaway reaction occurred at the gas-oxide interface.

The breakaway reaction, however, cannot be due to a direct formation of Fe_3O_4 from $3Cr_2O_3 \cdot Fe_2O_3$ in CO-CO_2 mixtures since it was also observed at a P_{CO_2}/P_{CO} value of 0.669, where FeO and not Fe_3O_4 is the stable iron

oxide [5]. The oxidation of $FeO \cdot Cr_2O_3$ to Fe_3O_4 and Cr_2O_3 was ruled out on the basis that the free energy for the reaction was 5730 cal/mole [6].

There was insufficient evidence to prove which reaction interface caused breakaway, but it is theorized that the phenomenon occurred in two steps: the protective oxide was thermally decomposed and a depleted alloy surface rich in iron was oxidized to Fe_3O_4 or FeO, depending on the gas composition. The presence of such a surface is discussed later.

If FeO was the high-temperature phase responsible for the oxidation curve shown in Fig. 7, then it also was a nonprotective oxide. Thus, gas compositions of CO and CO_2 containing CO_2 in amounts greater than that in equilibrium with Fe and FeO would be expected to eventually result in the breakaway phenomenon. The P_{CO_2}/P_{CO} values in equilibrium with Fe and FeO are those listed below [5]:

Temperature (°C)	P_{CO_2}/P_{CO}
427	1.35
538	1.07
649	0.75
760	0.58
871	0.48
982	0.40

At 982°C, the equilibrium value of P_{CO_2}/P_{CO} for these phases is 0.40, which is in agreement with the experimental value of 0.669.

Although the data presented demonstrated that the breakaway phenomenon occurred at 982°C and possibly at 935°C (see Fig. 6), this does not exclude the possibility that a similar phenomenon would occur at a lower temperature which would require a longer incubation period. If significance can be placed upon a critical weight gain of 1.8 mg/cm^2 above which the

breakaway occurred, it can be calculated that, for a CO_2 concentration of 0.24%, breakaway would occur after 1480 hr at 927°C, after 5900 hr at 871°C, after 15,700 hr at 816°C, and after 29,000 hr at 760°C. These times become less serious at the lower temperatures as far as the serviceability of the fuel element clad is concerned, but it is pointed out that weight gains in excess of about 0.3 mg/cm^2 would result in the spalling of the oxide when it is thermally cycled and that in service the oxide particles would be introduced into the high-velocity gas stream.

The reaction rates observed between type 304 stainless steel and CO_2 at 760°C decreased with increasing CO_2 pressure (Fig. 2), which is at variance with the observations of Draycott and Smith [4] and with the 982°C tests in this investigation. As will be recalled, the reaction product for times of 300 hr was $3Cr_2O_3 \cdot Fe_2O_3$, while in the tests of 800-hr duration (Table II) the reaction products were Fe_3O_4 and Cr_2O_3. It is believed that the presence of different reaction products was responsible for the difference between these results and those of Draycott's. Also, the present results at 760°C showed weight gains of between 0.2 and 0.3 mg/cm^2 (see Fig. 2 and Table II) for CO_2 pressures up to 0.24% (< 1 psi), while Draycott's results showed between 0.16 and 0.30 mg/cm^2 for pressures between 78 and 225 psi in the same temperature range.

The insensitivity of the reaction rates to various atmospheres of CO and CO_2 where the P_{CO_2}/P_{CO} ratios were less than 0.669 would be expected from the parabolic rates of oxidation. The equations for the rate curves, the weight gains, and the identification of the resulting oxide reaction products were not sensitive enough to delineate the effects of the gases,

as is apparent from the data shown in Table III. Usually, however, Arrhenius plots are able to reveal any differences in the reaction rates, as can be seen in Fig. 10. The curves in Fig. 10 show a decreasing temperature coefficient of reactivity as the CO content of the atmosphere was increased above about 843°C; below this temperature, the reverse effect was observed. As mentioned previously, inflections in the plots resulted from the appearance, disappearance, or change in the concentrations (thicknesses) of the various oxides. With the test at a P_{CO_2}/P_{CO} ratio of 0.12 the oxides above 843°C were principally the spinels and Cr_2O_3; below 843°C, the proportion of spinels was greater. The test at a P_{CO_2}/P_{CO} ratio of 0.043 showed the same oxides (Cr_2O_3 and Fe_3O_4) throughout the temperature range investigated, which would be expected since there was no change in the reaction rate constant. It appears therefore that high CO atmospheres stabilize Cr_2O_3 but do not favor the formation of the spinels.

The observance of Fe_3O_4 was unexpected, since its stability in a highly reducing atmosphere (with respect to iron) is questionable. Identification of Fe_3O_4 was somewhat difficult, since the spinels and Fe_3O_4 each had unit cell sizes ranging from 8.38 to 8.42 A. The conclusion that Fe_3O_4 was the reaction product was based on the spacings obtained by x-ray and electron diffraction patterns.

To account for Fe_3O_4 in the P_{CO_2}/P_{CO} ratios described above, it was possible that the atmosphere at the specimen surfaces was depleted in CO and therefore was not representative of the bulk gas stream. When iron sheet specimens were placed at the same specimen location as the stainless steel specimen, they remained bright after an 839-hr exposure to an atmosphere

in which the P_{CO_2}/P_{CO} ratio was 0.043, as would be expected if the atmosphere had remained unchanged.

Another possible explanation for the observation of Fe_3O_4 is based on the existence of a barrier between this oxide and the test atmosphere. The most logical barrier would be Cr_2O_3, which totally excluded Fe_3O_4 from the gases. Visual and metallographic evidence substantiated this interpretation. The origin of Fe_3O_4, however, was not accounted for.

Carburizing and Decarburizing Reactions in CO and CO_2

The variations in the carbon content of type 304 stainless steel with temperature exhibited a behavior that was characteristic for all gas compositions studied. In brief, there was a temperature range (about 600°C) below which carburization was not detected by the analytical method used (total combustion). At intermediate temperatures (600–900°C) all the gas mixtures, including CO_2, were carburizing and increased uniformly with temperature. Composition appeared to have but little effect in this temperature range. The effect of the atmosphere became significant at the highest temperatures investigated and either increased or decreased with temperature depending on the gas composition.

The reaction which accounts for carburization and decarburization of the alloy by the gases might be based upon the evidence that CO_2 is decarburizing and CO is carburizing in accordance with the following:

$$2CO \rightleftharpoons \underline{C} + CO_2$$

$$K = \frac{(A_C) \cdot P_{CO_2}}{(P_{CO})^2} \quad ,$$

from which

$$A_c = K\ (P_{CO})^2/P_{CO_2} \quad .$$

This reaction implies that the carbon should be in the metal and not in the oxide. Carbon analyses conducted on specimens from which the oxide was mechanically removed and compared with the carbon contents of specimens with the oxide intact showed in all cases a greater content of carbon when the oxide was removed, indicating that the carbon was not in the oxide. Additional support for the above reaction was that carbon deposits on the surfaces were not detected or observed.

The variations in the carbon content with temperature were attributed to the combined effects of reaction kinetics that increase with temperature and the parameter $(P_{CO})^2/P_{CO_2}$ that decreases with temperature increases. This would account for maximum carbon contents at the intermediate temperatures. The belief that carburization should increase with increases in the $(P_{CO})^2/P_{CO_2}$ ratio was verified by the data shown in Fig. 12.

The carbon contents of the specimens increased in the expected manner with increases in the $(P_{CO})^2/P_{CO_2}$ ratio up to a value of 0.227 (Fig. 14). Thereafter, further increases resulted in less carburization; this reversal in the carburization trend is most apparent in Fig. 13. The surface reactions responsible for this anomalous carburization behavior are not apparent from the available data. Since Cr_2O_3 was an effective barrier in preventing the reduction of Fe_3O_4 in an atmosphere high in CO content, it also may have served as a barrier for carbon diffusion. If this theory is correct, the oxidation reactions which promote the formation of Cr_2O_3 should simultaneously decrease the carburization reactions;

that is, carburization should decrease with the P_{CO_2}/P_{CO} ratio. For P_{CO_2}/P_{CO} values of 0.12 and 0.043 (Fig. 10), the corresponding $(P_{CO})^2/P_{CO_2}$ values are 0.372 and 0.879, respectively (Fig. 13).

For carbide particles to be absent at the metal surface (Figs. 15 and 17) in spite of the observed carbon increases, the surface would have to have been depleted in chromium. The presence of ferrite indicated that nickel was also depleted at the surface. It was concluded that the carbon introduced into the metal had not remained at the gas-oxide interface but had diffused inward to form chromium carbides. If carbon had been immobilized at the surface, pearlite instead of ferrite would have been observed.

SUMMARY

The oxidation, carburization, and decarburization reactions of type 304 stainless steel with CO_2 and CO-CO_2 atmospheres at concentrations between 0.00006 and 0.32% and temperatures between 425 and 982°C were investigated to establish a basis for the purification of the helium coolant of the Experimental Gas-Cooled Reactor and the framework for determining the effects of H_2, H_2O, and CH_4 in the presence of these two gases.

In atmospheres of CO_2 the oxide reaction products were $3Cr_2O_3 \cdot Fe_2O_3$, Fe_2O_3, Cr_2O_3, Fe_3O_4, and MnO. When CO was also present with CO_2, the surface layers observed were no longer oxides of iron but were Cr_2O_3 and oxide combinations having a spinel structure. The gas ratios in which these spinels were stable ranged between P_{CO_2}/P_{CO} values of 0.10 and 0.44. Gas compositions with P_{CO_2}/P_{CO} ratios equal to or less than 0.10 decreased

the proportion of the spinels and resulted in the formation of Cr_2O_3 and Fe_3O_4. In these cases, the Fe_3O_4 appeared to be surrounded by Cr_2O_3 rather than being present as a surface layer.

The oxidation rates of the alloy were governed mainly by the type of oxide being formed and the temperature. When Fe_3O_4 was the major surface reaction product, the oxidation rate was also dependent on the CO_2 pressure and the P_{CO_2}/P_{CO} ratio. Under these conditions the alloy oxidized at an accelerated rate after an incubation period, and Fe_3O_4 was not an adherent oxide but spalled upon cooling from the reaction temperature.

At a critical value of P_{CO_2}/P_{CO} (less than 0.44 to 0.67) the oxidation rates were insensitive to the concentration of CO and CO_2 and to their ratios above about 843°C. Below this temperature the oxidation rates increased as the P_{CO_2}/P_{CO} ratio was decreased. The alloy under these conditions oxidized according to the parabolic rate law and resulted in the formation of adherent oxide layers on the metal.

Carburization and decarburization occurred simultaneously with oxidation in a complicated manner that was dependent upon the carburizing potential $(P_{CO})^2/P_{CO_2}$ of the gas, upon the temperature, and upon the type of oxide that formed on the metal surface. Up to 600 to 700°C carburization was not measurable. Above this temperature carburization increased uniformly with temperature, reached a maximum value, then decreased with further temperature increases. The variations in the carbon contents of the alloy at a particular temperature increased with the $(P_{CO})^2/P_{CO_2}$ ratio up to a value of 0.227, then decreased with further increases in this ratio.

Metallographic, x-ray, and electron diffraction studies of the surface disclosed that nickel and chromium had been depleted from the alloy surface to depths as much as 0.003 in., resulting in the formation of ferrite and a carbide-free zone that appeared to have been decarburized but actually had been carburized. The oxidation reactions resulted in a maximum of 0.001 to 0.002 in. of grain boundary penetration and in a surface roughening which was more severe in the CO_2 atmospheres.

CONCLUSIONS

This study has shown that type 304 stainless steel was oxidized, carburized, and/or decarburized by all gas compositions investigated above 600°C. Below this temperature, surface reactions were insignificant. The oxidation reactions were governed by the P_{CO_2}, P_{CO_2}/P_{CO} ratios and the temperature, while the carburization and decarburization reactions depended upon the $(P_{CO})^2/P_{CO_2}$ ratio, temperature, and perhaps the P_{CO_2}/P_{CO} ratio.

With respect to the oxidation reactions, it was concluded that if the P_{CO_2}/P_{CO} ratios were maintained below those values unfavorable for the formation of FeO and Fe_3O_4, both the breakaway reaction and the oxide spalling could be controlled. Although the breakaway reaction can also be controlled by maintaining low CO_2 concentrations, the oxide spalling would not be eliminated and abrasive and radioactive particles would be introduced into the high-velocity helium coolant.

The carburization and decarburization reactions were significantly influenced by the chromium, in addition to the above variables. When chromium was oxidized to Cr_2O_3, it served as an efficient barrier to

prevent the reduction of Fe_3O_4 by CO and is believed to also be a barrier for carbon diffusion from the gas phases. Atmospheres which were either low or high in CO were less carburizing than those containing intermediate amounts of CO. Maximum carburization occurred at a $(P_{CO})^2/P_{CO_2}$ value of about 0.2.

From the standpoint of the purification of the helium coolant containing CO and CO_2, it was concluded that the concentrations would not have to be maintained below certain levels, but that proper gas ratios would be highly desirable in order to promote the formation of protective oxides such as Cr_2O_3. Since the carburizing potential of the gases is pressure-sensitive, ideally, the concentrations should be as low as practical but they could be in the range investigated.

Fortuitously, the gas conditions which appear most compatible with type 304 stainless steel are also those compositions which minimize the reactions with the graphite moderator and carbon steels [7].

ACKNOWLEDGMENTS

The author is indebted to the many service departments in carrying out various phases of these experiments. The assistance of T. E. Willmarth and R. M. Steele for the x-ray and electron diffraction analyses, the analyses performed by W. R. Laing and J. R. Sites of the Chemistry Division, and the metallographic work of W. R. Farmer proved to be necessary services in the interpretation of these experiments. The assistance of J. Newsome and J. Barnett in carrying out the experiments is appreciated.

Discussions of these results with J. H Frye, Jr., of the Metals and Ceramics Division and with E. E. Stansbury of the University of Tennessee were instrumental in the formulation of the conclusions reached in this investigation.

REFERENCES

1. J. C. Bockros and H. E. Shoemaker, Reactor Materials Compatibility with Impurities in Helium, GA-1508 (Jan. 12, 1961).

2. H. J. Pessl, Evaluation of Iron and Nickel Base Alloys for Medium and High Temperature Applications, HW-67715 (Feb. 1961).

3. J. C. Bockros and W. P. Wallace, The Oxidation of Metals by CO_2 at Temperatures of 1100–1740°F and Pressures of 1000–2000 psi, GA-700 (Mar. 25, 1959).

4. A. Draycott and R. Smith, Initial Results on the Compatibility of Austenitic Stainless Steels with Carbon Dioxide, AAEC/E52 (1960).

5. F. L. Harris, "Reactions Between Hot Steel and Furnace Atmospheres," Metals Progress 47, 84–89 (1945).

6. F. S. Boericke and W. M. Bangert, Equilibrium in the Reduction of Ferrous Chromite by Hydrogen and Energy Requirements in the Selective Reduction of Iron in Chromite, Bureau of Mines Report of Investigations 3813 (June 1945).

7. M. L. Becker, "Carburising and Graphitising Reactions Between Iron-Carbide Alloys, Carbon Monoxide and Carbon Dioxide," Journal of Iron and Steel Institute CXXI, 337–361 (1930–1931).

DISTRIBUTION

1. Biology Library
2–3. Central Research Library
4. Reactor Division Library
5. ORNL – Y-12 Technical Library, Document Reference Section
6–15. Laboratory Records
16. Laboratory Records, ORNL RC
17. ORNL Patent Office
18. G. M. Adamson
19. B. S. Borie
20. J. V. Cathcart
21. J. H. Coobs
22. J. E. Cunningham
23. J. H. DeVan
24. D. A. Douglas
25. J. H Frye, Jr.
26. A. E. Goldman
27. W. R. Grimes
28. W. O. Harms
29–31. M. R. Hill
32–36. H. Inouye
37. H. G. MacPherson
38. R. E. MacPherson
39. W. D. Manly
40. D. L. McElroy
41. C. J. McHargue
42. L. G. Overholser
43. P. Patriarca
44. J. L. Scott
45. G. M. Slaughter
46. A. M. Smith
47. E. E. Stansbury
48. W. C. Thurber
49. G. M. Watson
50. J. R. Weir
51–65. Division of Technical Information Extension (DTIE)
66. Research and Development Division (ORO)
67. H. E. Johnson
Dept. Mining and Metallurgy
University of Alberta
Edmonton, Alberta, Canada

68. W. L. Larsen
Iowa State University
Institute for Atomic Research
Box 14A, Station A
Ames, Iowa

69. H. J. Pessl
HAPO
Richland, Washington